4-2013

A Tunable Miniaturized RF MEMS Resonator With Simultaneous High Q (500-735) and Fast Response Speed (< 10-60 mu s)

Joshua A. Small
Birck Nanotechnology Center, Purdue University, jsmall03@purdue.edu

Muhammad Shoaib Arif
Birck Nanotechnology Center, Purdue University, marif@purdue.edu

Adam Fruehling
Birck Nanotechnology Center, Purdue University, soimems@purdue.edu

Dimitrios Peroulis
Birck Nanotechnology Center, Purdue University, dperouli@purdue.edu

A Tunable Miniaturized RF MEMS Resonator With Simultaneous High Q (500–735) and Fast Response Speed $(< 10 - 60\ \mu s)$

Joshua Small, *Member, IEEE*, Muhammad Shoaib Arif, *Student Member, IEEE*, Adam Fruehling, *Student Member, IEEE*, and Dimitrios Peroulis, *Member, IEEE*

***Abstract*—This paper reports on the design, fabrication, and measurement of a novel radio frequency (RF) microelectromechanical systems (MEMS) tunable all-silicon evanescent-mode cavity-based resonator that simultaneously achieves high quality factor and fast response speed. The resonator is based on a 1.5-mm-deep silicon-etched cavity attached to a gold-coated silicon substrate with an array of 75 185-μm-long 20-μm-wide 1-μm-thick gold beams. The 54-mm^3 resonator is tunable from 15.2 GHz up to 16.5 GHz (analog tuning range) and up to 17.8-GHz range (digital tuning range) with an array of 75 MEMS fixed–fixed beams. The MEMS beams are biased against their own silicon substrate. This helps keep RF leakage at a minimum and permits high quality factors of 500–735 for the all-silicon configuration. By applying dynamic biasing waveforms, the MEMS tuners respond within 9 μs (actuation time) and 60 μs (release including settling time). To the best of the authors' knowledge, the presented resonator is more than 3$\times$ smaller, achieves nearly 30% higher average quality factor, and is at least 10–100$\times$ faster than state-of-the-art resonators based on similar technology, implemented in similar frequency ranges. [2012-0122]**

***Index Terms*—Evanescent-mode cavity, microelectromechanical systems (MEMS), micromachining, silicon cavity, switching time, tunable filter, tunable resonator.**

I. Introduction

LOW-LOSS widely tunable radio frequency (RF) front-end filters are particularly desirable in tunable transceivers in both commercial and department-of-defense systems. Over the last five years, there have been several successful demonstrations of low-loss widely tunable RF microelectromechanical systems (MEMS) resonators and filters using the evanescent-mode cavity-based implementation. Evanescent-mode cavities offer a good balance between filter size, loss, spurious-free range, and tuning range [1]–[4].

Frequency tuning in these cases has been achieved using either piezoelectric [1]–[4] or electrostatic MEMS actuators [5]–[13]. Piezoelectrically tuned resonators yield excellent RF results. However, such tuners are typically large with diameters on the order of 12.7 mm [1] and typically have slow response speeds on the order of 1 ms. Electrostatically tuned resonators can be made smaller and thus faster [6], [7], [13]. In all these designs, however, there is an inherent tradeoff between resonator volume, Q_u, frequency tuning, and tuning speed. Liu *et al.* [7] demonstrated resonator cavities with a volume of 509 mm^3 tuned with 7-mm MEMS diaphragms and achieved a 2.6 : 1 (1.9–5 GHz) tuning range and $Q_u = 300-650$, but with a slow response speed of 300–500 μs (not reported directly but inferred from movable tuner size). Park *et al.* [6] employed cavities with a volume of approximately 700 mm^3 and achieved a similar tuning range (4.07–5.58 GHz) with much improved speed on the order of 60–130 μs [19]. This was accomplished by utilizing 138-μm-long 60-μm-wide 4-μm-thick MEMS beams. The quality factor of these resonators though was limited to $Q_u = 300$–500 due to the necessary MEMS biasing network. The biasing network penalty on the resonator quality factor is over 50% since their inherent Q_u could be increased to 1000 if the biasing network was eliminated. Stefanini *et al.* [13] employed a 180-mm^3 resonator with an improved biasing network and was able to achieve $Q_u = 400$–550 with MEMS beams with a continuous tuning range of 11.9–13.6 GHz (11.9–14.2 GHz was the digital tuning range). The employed MEMS beams were 1.1-mm-long highly deflected cantilever beams with an estimated response speed on the order of 200–300-μs actuation time and > 1000-μs release/settling time (not directly reported but inferred from movable tuner size).

A potential means by which to improve the electromechanical response without compromising the RF performance is to divide the solid diaphragm into small MEMS fixed–fixed beams whose biasing network remains outside of the RF cavity. Furthermore, when compared to MEMS tuning diaphragms, the proposed technique is less susceptible to shock, acceleration, and vibration due to the four-orders-of-magnitude reduced mass (MEMS diaphragm mass of 8.2×10^{-7} kg; MEMS bridge mass in this work is 2.83×10^{-11} kg) [12].

Manuscript received May 7, 2012; revised August 26, 2012; accepted October 11, 2012. Date of publication November 21, 2012; date of current version March 29, 2013. This work was supported in part by the Defense Advanced Research Projects Agency under the Purdue Microwave Reconfigurable Evanescent-Mode Cavity Filters Study and in part by the National Nuclear Security Association Center of Prediction of Reliability, Integrity and Survivability of Microsystems and Department of Energy under Award DE-FC5208NA28617. Subject Editor F. Ayazi.

J. Small was with the School of Electrical and Computer Engineering and the Birck Nanotechnology Center, Purdue University, West Lafayette, IN 47907 USA. He is now with the School of Electrical and Computer Engineering, University of California, Davis, CA 95616 USA (e-mail: jasmall@ucdavis.edu).

M. S. Arif, A. Fruehling, and D. Peroulis are with the School of Electrical and Computer Engineering and the Birck Nanotechnology Center, Purdue University, West Lafayette, IN 47907 USA (e-mail: marif@purdue.edu; adam.fruehling@gmail.com; dperouli@purdue.edu).

Color versions of one or more of the figures in this paper are available online at http://ieeexplore.ieee.org.

Digital Object Identifier 10.1109/JMEMS.2012.2226928

The authors recently experimentally demonstrated the potential of this technique in a 113-mm^3 resonator tunable between 10.7 and 11.1 GHz (analog range) and up to 13 GHz (digital range) with $Q_u = 593$–1077 [14] and response speed of 82 μs (actuation time) and 112 μs (release/settling time). While this was state-of-the-art performance, this paper presents a miniaturized resonator with more than 50% volume reduction and significantly improved overall performance: 8.2% analog tuning range, 9-μs actuation time, 60-μs release/settling time, and 11.4/mm^3 average quality factor per resonator volume. These represent $> 2.2\times$ improved analog tuning range, $> 9\times$ faster actuation time, $1.8\times$ faster release/settling time, and $>50\%$ higher quality factor per resonator volume compared to the authors' previous work [14]. These significant improvements are attributed to two key advancements presented for the first time: 1) all-silicon resonator technology with an array of 75 tuning MEMS beams and b) dynamic biasing waveforms that optimize the response speed of the MEMS tuners. The following sections summarize the design, fabrication technology, and measured results that demonstrate the aforementioned performance.

II. Design

Fig. 1(a) shows the complete all-silicon tunable resonator cavity. The resonator is fed by a shorted coplanar waveguide (CPW) transmission line. An array of substrate-biased RF-MEMS fixed–fixed beams is designed to be directly over the post. Deflecting the beams away from the post results in a resonant frequency shift of the resonator. Substrate biasing, as shown in Fig. 1(c), is used in order to reduce RF leakage by not interfering with the RF current path. The device design details for the tunable resonator are explained further in the following sections.

A. RF Design

A Ku-band tunable resonator with $Q_u > 700$ and frequency tuning of $> 20\%$ is designed to demonstrate the proposed concept. The frequency tuning is limited to 20% in order to achieve < 10-μs switching time. In this band, the skin depth of gold is $0.72 - 0.59\mu$m. The beams are designed to be at least 1 μm thick such that the Q_u is not severely degraded. Since the cavities are considered highly loaded, the capacitive region between the post and the ceiling is the primary determining factor of the operation frequency. The post diameter is chosen to be 240 μm in order to achieve Ku-band operation. The cavity depth is designed to be 1.5 mm in order to achieve the specified $Q_u > 700$ across the tuning frequency band. While deeper cavities will result in higher Q_u, several applications need substrate thicknesses in the 1–2-mm range. The capacitive gap between the ceiling and the post is chosen to be 5–6 μm in order to have the initial resonant frequency be within the specified Ku-band. Closer gaps have been successfully demonstrated in the literature [4]. A 5–6-μm capacitive gap represents a compromise between frequency tuning and repeatability. The fixed–fixed beams are designed with $w_b = 20$ μm (fixed–fixed beamwidth), $L_b = 185$ μm, and an actuation dc gap $g_{\rm dc}$ of 4 μm in order to achieve $> 20\%$ frequency tuning.

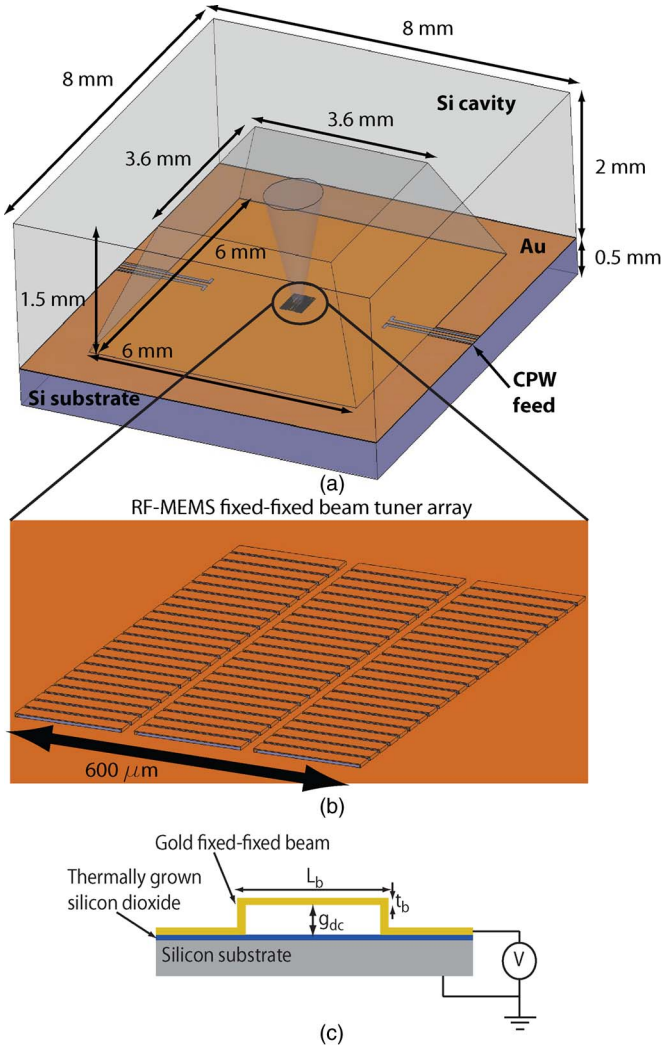

Fig. 1. Schematics of the proposed RF-MEMS tunable all-silicon cavity-based resonator. (a) Overall 3-D perspective of the presented resonator. (b) Close-up view of the array of resonator tuners under the evanescent post. (c) Two-dimensional biasing schematic with device parameters of the substrate-biased MEMS tuners.

Fig. 2 shows the full-wave numerical simulation of the expected RF performance per the device parameters listed in Table I. A frequency tuning of 20% is expected for an initial RF gap (capacitive gap between the tuners and post) g_{RF} of 5 μm between the evanescent post and MEMS fixed–fixed beam array for a beam deflection of 4 μm. Quality factors from 675 to 825 are expected.

B. Impact of Series Resistance on Q_u

The series resistance of the resonator can have a significant impact on the unloaded quality factor. The following analytical expression from [15] shows the relationship between the Q_u and the resonator design specifications:

$$\frac{1}{Q_u} = \frac{R_s}{2\pi f_0 \mu_e}\left(\frac{\left(\frac{1}{a}+\frac{1}{b}\right)}{ln\left(\frac{b}{a}\right)} + \frac{2}{h}\right) \tag{1}$$

where R_s is the series resistance of the resonator, f_0 is the operation frequency of the resonator, μ_e is the permeability, a is the radius of the post, b is the radius of the cavity, and h is the depth

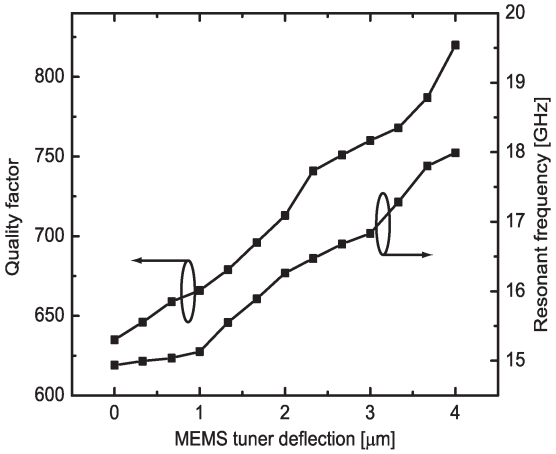

Fig. 2. Simulated frequency tuning and unloaded quality factor of the proposed RF-MEMS tunable all-silicon cavity-based resonator. (Please see Fig. 1 for the geometry description.)

TABLE I
FINAL DESIGN PARAMETERS OF ALL-SILICON RF-MEMS TUNABLE RESONATOR

Parameter	Value
Beam length: L_b (μm)	185
Beam width: w_b (μm)	20
Beam thickness: t_b (μm)	0.9
DC gap: g_{dc} (μm)	4
Pull-down voltage: V_{pd} (V)	77
Effective tuner mass: m_{eff} (kg)	2.83×10^{-11}
Mechanical resonant frequency: f_{m0} (kHz)	26
Mechanical quality factor: Q_m	32
Switching time: t_{pd} (μs)	12–21
Evanescent post diameter: $\varnothing_{post}$ (μm)	240
Initial capacitive gap: g_{RF} (μm)	5
Silicon cavity depth (mm)	1.5
Frequency tuning range (GHz)	15–18
Electromagnetic unloaded quality factor: Q_u	675–825

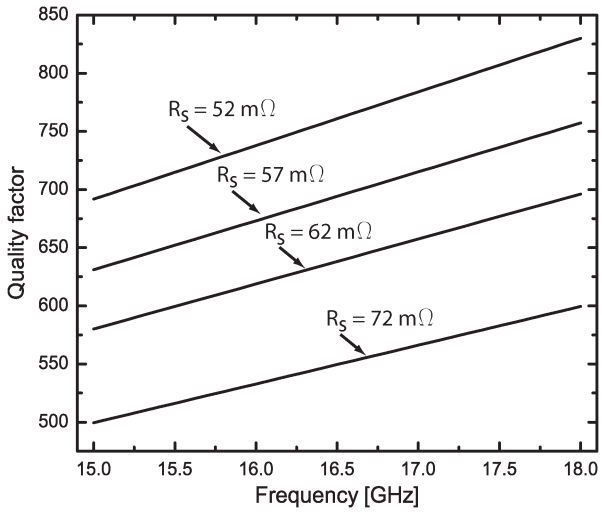

Fig. 3. Calculated Q_u versus frequency for various values of series resistance R_s.

of the cavity. Fig. 3 shows the impact of series resistance on Q_u. A substantial impact in Q_u of a few 100 points is observed for a mere change in R_s of tens of milliohms. Therefore, care must be taken in choosing the appropriate integration technique that will result in the lowest series resistance in order to approach the simulated Q_u values.

C. Pull-Down Switching Time

The fixed–fixed beams are designed to achieve switching times on the order of tens of microseconds while balancing the inherent tradeoffs with tuning range and Q_u. In order to achieve the desired switching time, the fixed–fixed beams are designed to be underdamped. The damping b of a rectangular or circular parallel-plate geometry can be expressed as [16]

$$b = \frac{3}{2\pi}\frac{\mu_m A^2}{g_{\rm dc}^3} \tag{2}$$

where A is the area of the MEMS membrane $(w_b \times L_b)$, $g_{\rm dc}$ is the gap between the fixed–fixed beam and the nearest damping surface, and μ_m is the coefficient of viscosity. At standard atmospheric temperature and pressure, μ_m is 1.845×10^{-5} kg/m $\cdot$ s [16]. The mechanical quality factor Q_m of a fixed–fixed beam can be approximated by the following expression [16]:

$$Q_m = \frac{\sqrt{E\rho}t_b^2}{\mu_m\left(\frac{w_b L_b}{2}\right)^2} g_{\rm dc}^3 \tag{3}$$

where E is the Young's modulus of the beam material and ρ is the density of the beam material. The mechanical resonant frequency f_{m0} can be found as a function of b and Q_m

$$f_{m0} = \frac{1}{2\pi}\frac{k}{bQ_m}. \tag{4}$$

The tunable resonator presented in this paper is designed to have $g_{\rm dc} = 4$ μm. This value represents a compromise between frequency tuning and switching time. The beam parameters are $L_b = 185$ μm, $w_b = 20$ μm, $t_b = 0.9$ μm, residual mean stress σ of 10 MPa, spring constant k of 10 N/m, and effective mass m_{eff} of 2.83×10^{-11} kg ($m_{eff} = 0.44\rho t_b w_b L_b$). Based on these parameters, the b, Q_m, f_{m0}, and pull-down voltage V_{pd} ($V_{pd} = \sqrt{8kg_{\rm dc}^3/27\epsilon_0 w_b L_b}$) are calculated to be 1.8843×10^{-6} kg/s, 32, 26 kHz, and 77 V, respectively. The bridges can be designed for high power handling (1–10 W) applications by simply increasing the spring constant. However, this design tradeoff may result in higher tuning voltage.

Since the fixed–fixed beams have a relatively small damping coefficient and $Q_m \geq 2$, they fit the criteria of an inertia-limited system. As a result, we can use the following closed-form solution for the pull-down switching time [16]:

$$t_{pd} = 3.67\frac{V_{pd}}{2\pi V_{\rm app} f_{m0}} \tag{5}$$

where $V_{\rm app}$ is the actual applied voltage that, in most cases, is 1.2–1.4V_{pd} in order to obtain good switching time. Fig. 4 shows the calculated switching time for the pull-down states. It is observed that the pull-down states have switching times on the order 10–21 μs for $t_b = 1$ μm and $V_{\rm app} = 77$–154 V. It is also seen that, by simply increasing the thickness of the fixed–fixed beam, the switching time improves to < 10 μs.

The penalty for utilizing an underdamped beam design is a long release switching time of > 1 ms. This is expected due to the near lack of squeeze film damping, resulting in a relatively high Q_m. The long settling time will not only be experienced on the release switching time from the down-to-up state but also on the analog states before the beam snaps down

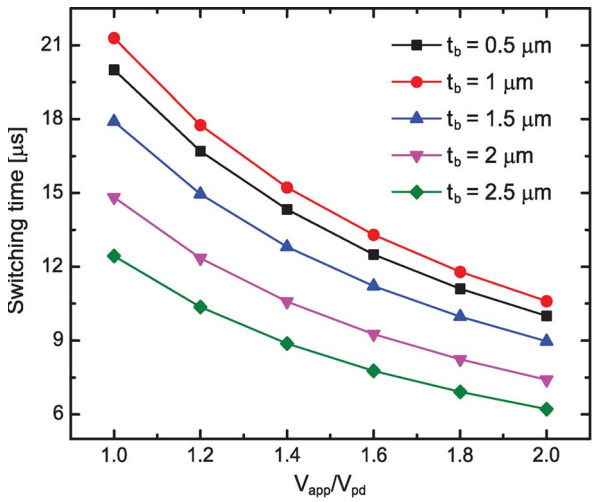

Fig. 4. Calculated switching time for pull-down states for various beam thicknesses; $w_b = 20$ μm, and $L_b = 185$ μm.

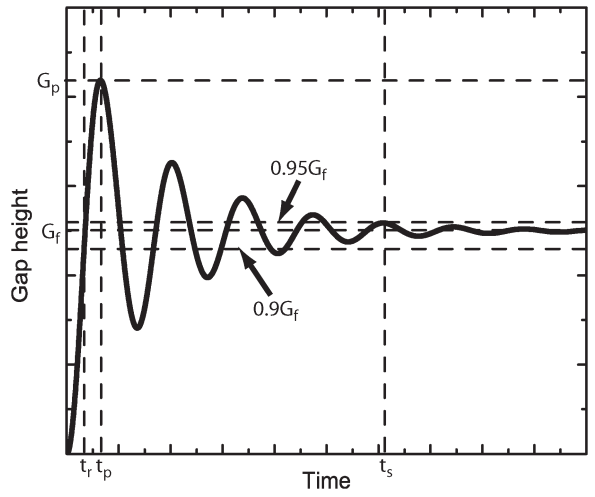

Fig. 5. Sketch of typical underdamped second-order system response to a unit-step input. Key metrics are noted: Peak gap G_p, final gap G_f, rise time t_r, peak time t_p, and settling time t_s.

to the substrate. Employing dc-dynamic biasing waveforms may potentially improve the settling time.

D. DC-Dynamic Biasing

The rise time of a typical unit-step bias is on the order of hundreds of nanoseconds. This very fast rise time will evoke the well-known underdamped second-order step response from the MEMS fixed–fixed beams of this resonator. Fig. 5 shows the key metrics of an underdamped second-order system in response to a unit-step input. This ringing will be experienced on the analog gap heights before the pull-in gap height and after releasing the beam from the down-to-up state. The metrics are as follows: final gap height G_f, peak gap height G_p, rise time t_r, peak time t_p, and settling time t_s. Typically, t_r is defined as the time that it takes to get from $0.01G_f$ to $0.9G_f$, and t_s is defined as the time that it takes to get within 5% of G_f. The settling time for the proposed beams in this paper is $\sim$1 ms. If, however, we input a bias with a rise time that is longer than the magnitude of t_r and t_p (unit-step input is 1–2 orders shorter), we anticipate the beams to behave much more quasistatically and reach the steady-state gap in a shorter period of time.

TABLE II
CALCULATED TIME PARAMETERS OF DC-DYNAMIC WAVEFORM

t_1	t_2	t_3	t_4
0 μs	60 μs	1 ms	1.06 ms

We begin by expressing the key underdamped response metrics as a function of the beam geometrical parameters Q_m. First, the damping ratio ζ is expressed as

$$\zeta = \frac{b}{2m_{eff}\omega_{m0}}. \tag{6}$$

We can relate ζ to Q_m by the following:

$$\zeta = \frac{1}{2Q_m}. \tag{7}$$

The percent overshoot $\%OS$ can now be expressed in terms of Q_m

$$\%OS = 100 \times e^{\frac{-\zeta\pi}{\sqrt{1-\zeta^2}}} = 100 \times e^{\frac{-\frac{\pi}{2Q_m}}{\sqrt{1-\left(\frac{1}{2Q_m}\right)^2}}}. \tag{8}$$

We can express t_r as

$$t_r = \frac{2.16\left(\frac{1}{2Q_m}\right) + 0.6}{\omega_{m0}}. \tag{9}$$

The t_p can be expressed as follows:

$$t_p = \frac{\pi}{\omega_{m0}\sqrt{1-\zeta^2}} = \frac{\pi}{\omega_{m0}\sqrt{1-\left(\frac{1}{2Q_m}\right)^2}}. \tag{10}$$

Finally, we can calculate t_s (5% of steady-state value) as a function of Q_m

$$t_s \approx \frac{3}{\zeta\omega_{m0}} \approx \frac{6Q_m}{\omega_{m0}}. \tag{11}$$

For a fixed–fixed beam with $Q_m = 32$ and $f_{m0} = 26$ kHz, $t_p = 19$ μs, $t_r = 4$ μs, $t_s = 1.2$ ms, and $\%OS = 95.2$. Consequently, the rise time of the input bias is chosen to be at least 50–60 μs in order to achieve a quasistatic beam behavior. Under quasistatic behavior, the beam does not exhibit significant steady-state gap height overshoot and ringing as in the dynamic case. Also, this down-to-up switching time is typical for the more traditional critical and overdamped MEMS beam designs. A detailed study that expands upon the theoretical development and experimental validation of the dc-dynamic biasing waveform can be found in [17].

Fig. 6 shows the typical response of a fixed–fixed beam to an input dc-dynamic (with an approximate rise and decay) biasing waveform. The dynamic rise time t_e as described in the previous paragraph is chosen to be at least $\sim 2.5 \times t_p$. The times t_1 and t_3 are user defined; however, $t_2 - t_1 = t_e$, and $t_4 - t_3 = t_e$. The voltage V_f is the voltage needed to obtain the steady-state gap height G_f. The V_0 voltage corresponds to the G_0 gap height. Table II shows the calculated timing parameters for an example dc-dynamic waveform based on Fig. 6.

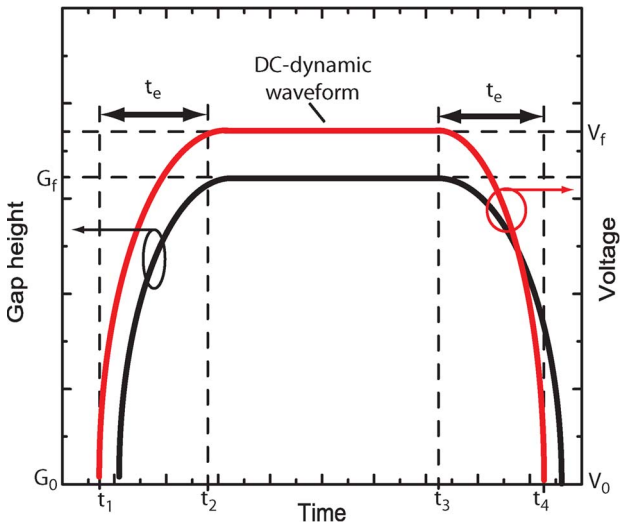

Fig. 6. Sketch of typical fixed–fixed beam response to an input dc-dynamic biasing waveform.

E. Overall Tunable Resonator Performance

Based on the electromagnetic and electromechanical design, a figure of merit can be developed to rate the overall performance of the entire resonator. We propose the following expression:

$$\text{F.O.M.} = \frac{Q_{\text{avg}}\Delta f}{V_{\text{cavity}} m_{\text{tuner}} V_{\text{tune}} t_{\text{avg}}} \tag{12}$$

where Q_{avg} is the average resonator Q_u, Δf is the frequency tuning, V_{cavity} is the volume of the resonator cavity, m_{tuner} is the mass of the tuning mechanism, V_{tune} is the voltage needed to cover the frequency tuning range, and t_{avg} is the average switching time of the resonator. Table IV shows a quantitative comparison between this and previous work. The proposed tunable resonator in this work has a 68× improvement in F.O.M. when compared to the authors' previous work.

III. Fabrication and Assembly

Fig. 7 summarizes the fabrication sequence for the MEMS fixed–fixed beam tuner array. The fixed–fixed beams are fabricated on a high-resistivity silicon substrate (~ 10 k$\Omega - $ cm) with a thickness of 525 μm and 0.2 μm of thermally grown SiO_2. The fabrication begins with spin coating and patterning a 20-μm-thick AZ9260 photoresist layer to serve as a liftoff layer for copper. Copper and a thin titanium adhesion layer (< 20 nm) are flood deposited on the liftoff mold to ~ 7 μm thick. To facilitate the liftoff process, the sample is placed in an ultrasonic cleaner with acetone. This thick copper metalization defines the highly loaded capacitive gap g_{RF} between the fixed–fixed beam array and the evanescent post. Next, 2 μm of gold is flood deposited and patterned to form the shorted CPW feed lines, anchor points, and openings in the metal to permit dc biasing between the fixed–fixed MEMS bridge and the silicon substrate. A very thin (< 20 nm) titanium adhesion layer is also included. Next, a 4-μm-thick SC1827 photoresist sacrificial layer is coated and patterned. Gold is again flood deposited to 1 μm thick and patterned for the MEMS fixed–fixed beam tuners. Again, a very thin (< 20 nm) titanium adhesion layer is also included. Finally, the MEMS fixed–fixed beam tuners are released in a standard photoresist stripper, and the sample is dried in a CO_2 critical point dryer. Fig. 8 is a SEM of a typical fabricated fixed–fixed beam MEMS tuner array.

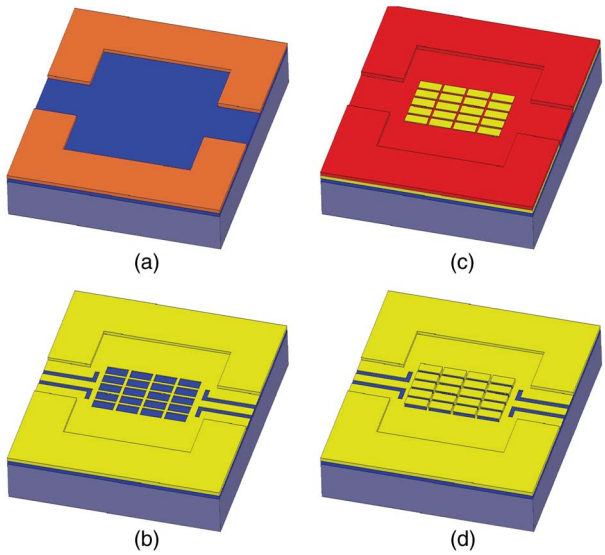

Fig. 7. Fabrication process of MEMS fixed–fixed beam tuner array. (a) Liftoff of thick Ti/Cu ring to define the capacitive RF gap between the evanescent post and RF-MEMS fixed–fixed beam tuner array. (b) Flood sputter deposition and patterning of Ti/Au for CPW feed line and electric field openings for beam actuation. (c) Photoresist sacrificial layer, flood sputter deposition, and patterning of Ti/Au to define the RF-MEMS fixed–fixed beam tuner array. (d) Photoresist sacrificial layer etched in photoresist stripper and samples dried in CO_2 critical point dryer.

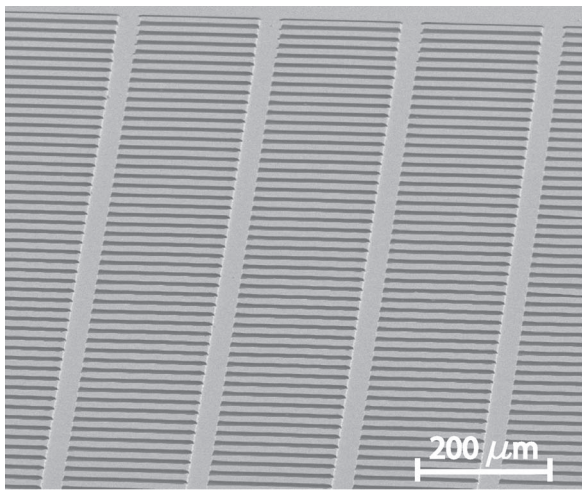

Fig. 8. Scanning electron micrograph of typical MEMS fixed–fixed beam tuner array.

Fig. 9 summarizes the fabrication sequence for the silicon cavity. We start with a 2-mm-thick high-resistivity silicon wafer (~ 10 k$\Omega \cdot$ cm) that is coated with 300 nm of low pressure chemical vapor deposition (LPCVD) silicon nitride. The silicon nitride is patterned through dry etching with SF_6 in a reactive ion etcher. The silicon nitride serves as a wet etch mask for the subsequent silicon etch. The silicon is wet etched 1.5 mm deep in a 45% KOH by volume solution maintained at 80 °C. The etch rate is ~ 55 μm/h. Next, the silicon nitride layer is stripped in hot phosphoric acid. Finally, the cavity is flood deposited with 2 μm of gold.

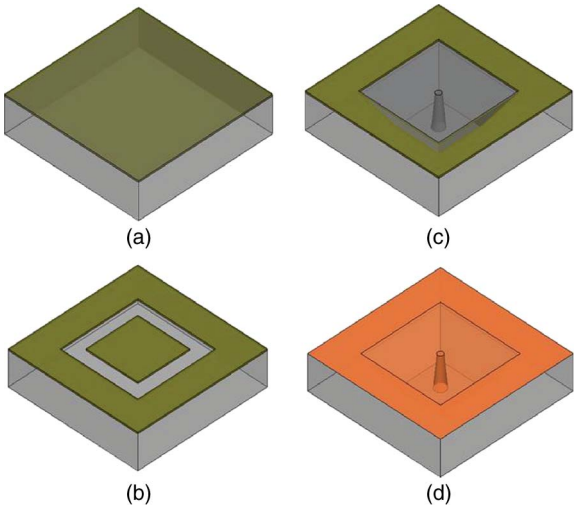

Fig. 9. Fabrication process of silicon resonator cavity. (a) High-resistivity thick silicon wafer with LPCVD silicon nitride. (b) Pattern silicon nitride with dry SF_6 reactive ion etch to form the silicon cavity wet etch mask. (c) Wet etch of silicon in KOH. (d) Flood sputter deposition of Ti/Au.

The MEMS die and the silicon cavity are integrated with a mechanical pressure bond. Fig. 10 shows each module of the all-silicon tunable resonator. The fixture dimensions are $2.25 \times 5 \times 1.5$ cm^3. The large fixture dimensions were chosen in order to measure the resonators quickly and be able to assemble and disassemble them quickly as well. In addition to holding the cavity and MEMS die together, the fixture facilitates dc biasing of the MEMS die. The backside of the silicon substrate is exposed and electrically connected to the biasing plate through a metallic spring. This technique greatly simplifies the dc biasing efforts when considering that the fixed–fixed beam MEMS tuner array side needs to be faced up in order for the RF probes to access the shorted CPW feeds (Please refer to Fig. 1 for a geometry description). Fig. 11 shows how the all-silicon resonator is simultaneously measured and dc biased.

IV. Results and Discussion

A. RF Measurements

The RF measurements are done using an Agilent programmable network analyzer and 2.4-mm GSG RF probes by Cascade Microtech. Fig. 12 shows the measured frequency tuning of the MEMS tunable all-silicon cavity resonator. The resonator is designed to be weakly coupled for the accurate extraction of Q_u. We obtained numerical values for Q_u by dividing the center frequency by the 3-dB bandwidth. A measured quality factor of 500–735 from 15.2–17.8 GHz for applied biases of 0–77 V is demonstrated. A consequence of using traditional RF-MEMS tuners is that the resonator has two analog regions and one digital region. The digital response can be completely eliminated by deploying actuation techniques like leveraged bending [18] to extend the travel range of the MEMS bridges, thereby improving the frequency tuning range. In addition, the initial RF gap can be decreased through careful process characterization to further improve the frequency tuning.

Fig. 13 shows the measured and the simulated unloaded quality factor versus frequency. The measured quality factor is

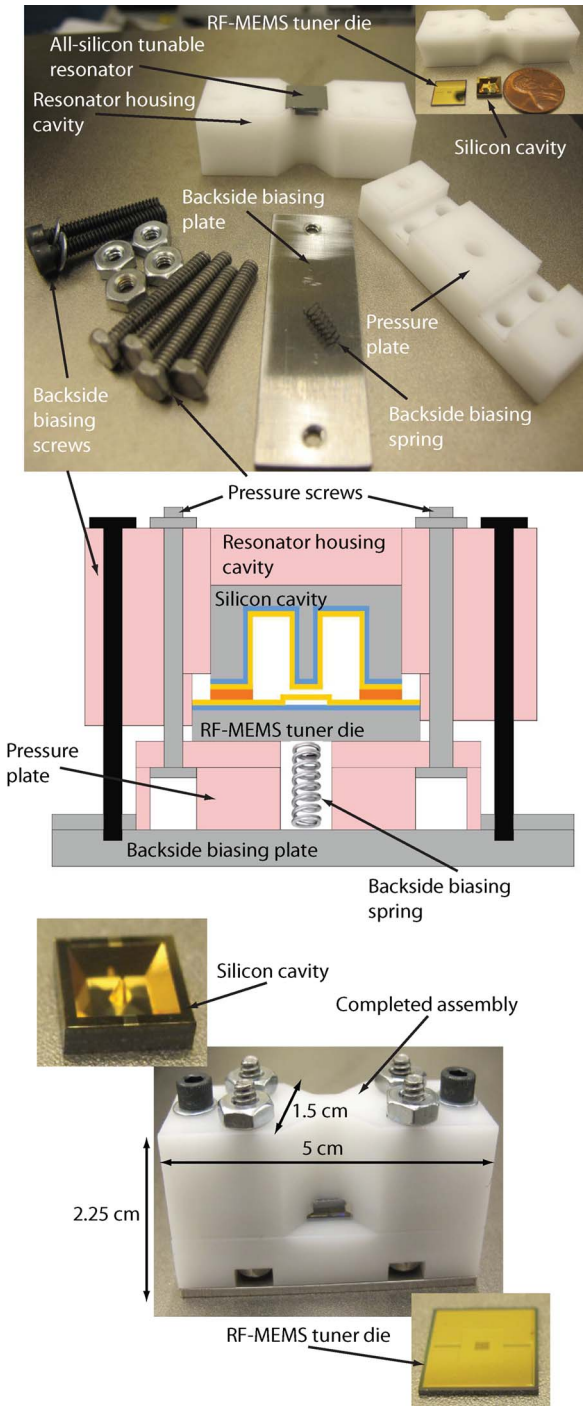

Fig. 10. Individual parts and completed assembly in test fixture.

within 75%–85% of the simulated quality factor. The suspected mechanism of loss is the voids between the interface of the cavity and the MEMS die. As described in Section II-B, the imperfect interface will add series resistance that will reduce the quality factor (please refer to Fig. 3). With careful fixture design that applies a balanced pressure on the MEMS die, the measured quality factor is expected to exceed 90% of the simulated result across the entire frequency tuning range.

The smoothness and flatness of the metal layers and the silicon surfaces is the key in permitting the measured performance to approach the ideal simulated performance. Silicon micromachining and dc magnetron sputter coating provide

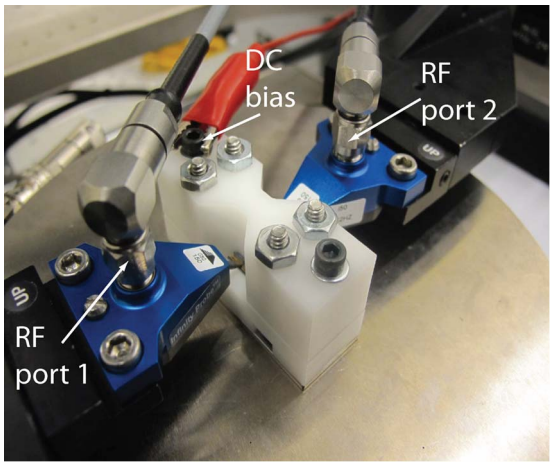

Fig. 11. Measurement in progress of all-silicon tunable cavity.

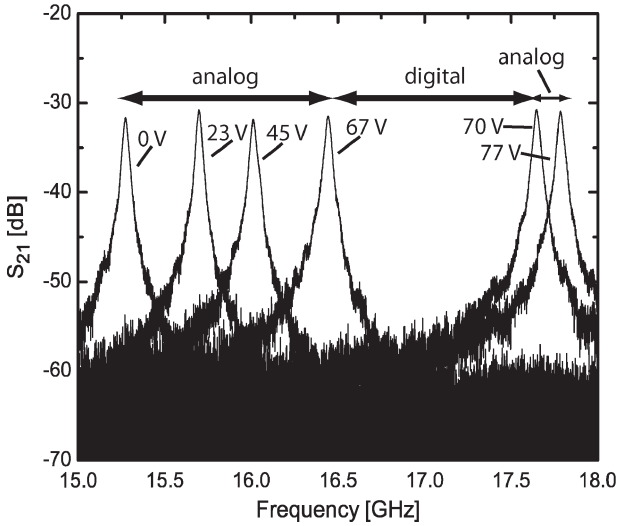

Fig. 12. Measurement of frequency tuning of MEMS tunable all-silicon cavity resonator.

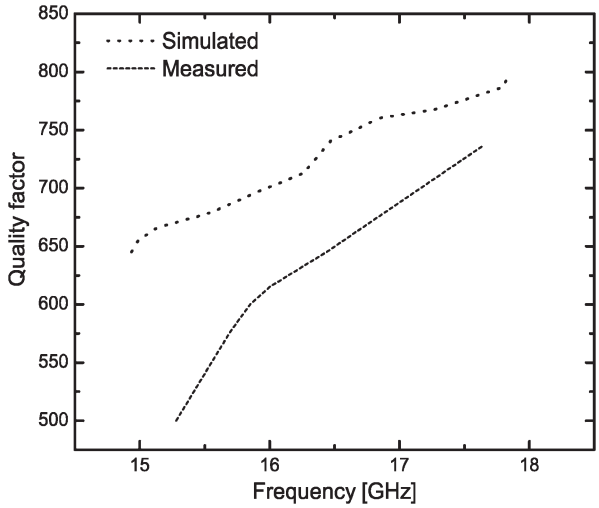

Fig. 13. Measurement of quality factor compared to simulation.

mirrorlike surfaces that closely resemble the ideal surfaces used in full-wave numerical simulation. Furthermore, the copper ring that defines the gap between the post and the fixed–fixed beam MEMS tuner array is sputtered as opposed to electroplated. The smoothness provided by the dc magnetron sputtering process

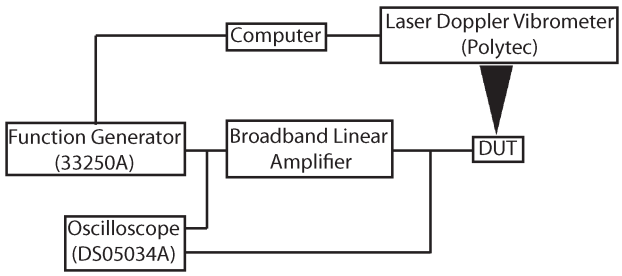

Fig. 14. Measurement setup for switching time.

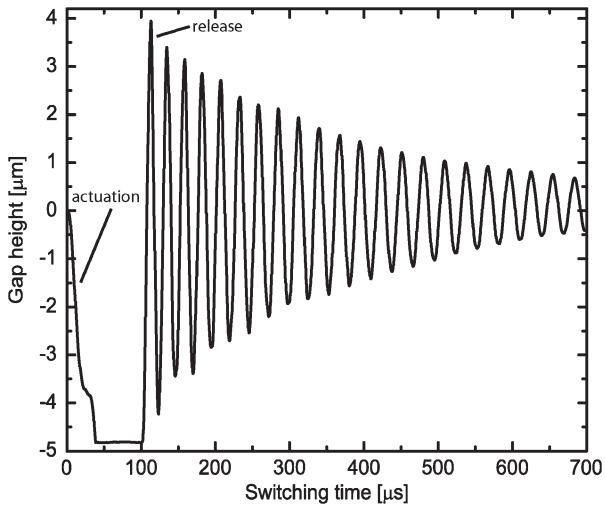

Fig. 15. Total switching time response for a unit-step input bias of 67 V.

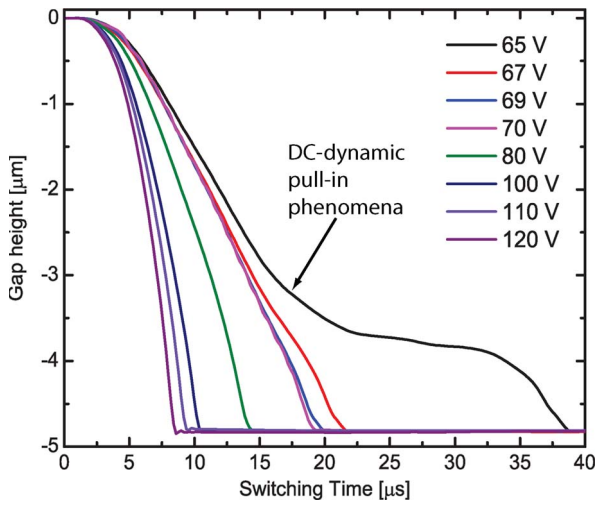

Fig. 16. Close-up measurement of pull-down switching time for a unit-step input bias.

TABLE III
CALCULATED AND MEASURED SWITCHING TIME OF MEMS FIXED–FIXED BEAM TUNERS

V_{app} [V]	Calculated Time [μs]	Measured Time [μs]
67	21.12	22
69	20.05	20
70	20.21	19
80	17.68	15
100	14	11
110	12	10
120	11.7	9

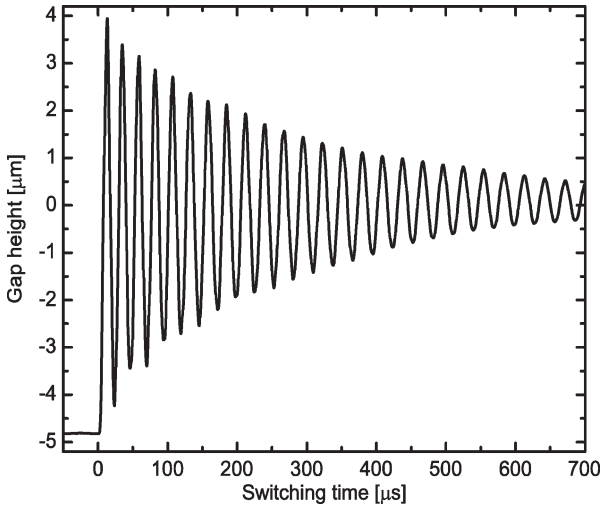

Fig. 17. Close-up of release time measurement with laser Doppler vibrometer measurement of gap height versus switching time of an isolated beam. Unit-step bias is illustrated.

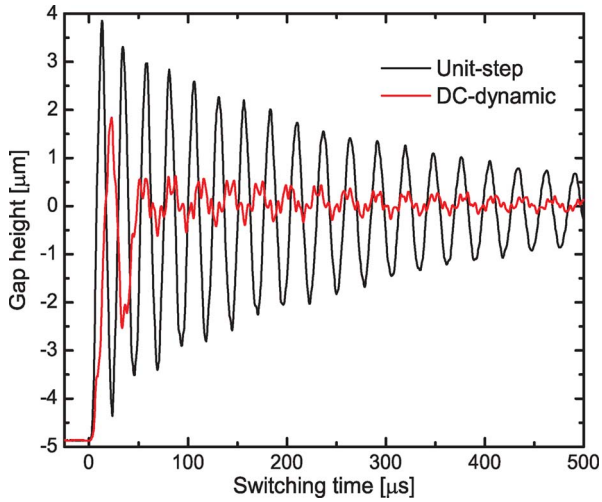

Fig. 18. Measured pull-down and release time versus gap height of single RF-MEMS fixed–fixed beam tuner. Response for both unit-step and ramped input biases is illustrated.

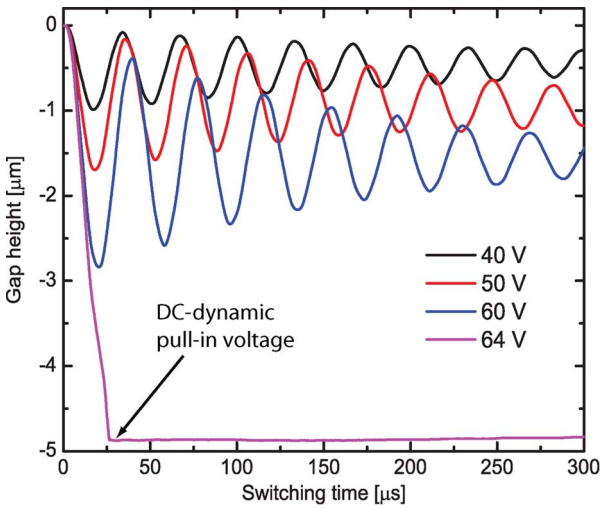

Fig. 19. Measurement of pull-down switching time for beam in analog gap region for a typical unit step for various applied biases.

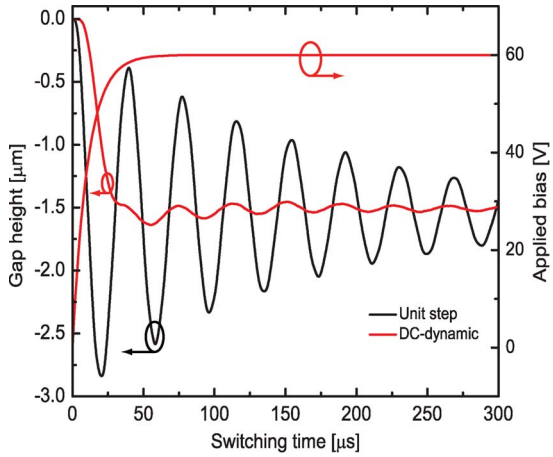

Fig. 20. Close-up of actuation measurement with laser Doppler vibrometer measurement of gap height versus switching time of an isolated beam at 60 V. Unit-step and dc-dynamic input biases are illustrated.

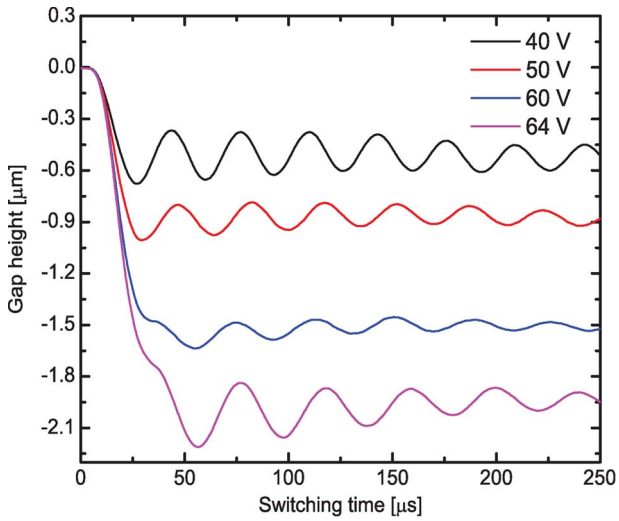

Fig. 21. Measurement of actuation switching time for multiple gaps in the analog gap region with the dc-dynamic applied bias.

reduces the likelihood of severe current crowding. Like the other highlighted process advantages, the sputtered copper ring mimics the simulated device surfaces quite well. Finally, when compared to Au and Cu electroplating, the sputtered films reduce process uncertainty due to the improved uniformity of the thin film layer from die to die. A nonuniform metal thickness will add a tilt component to the initial RF gap between the post and the tuners. This can lead to a decreased frequency tuning range due to the $g_{\rm dc}^{-1}$ dependence.

B. Measured Pull-Down Switching Time

The electromechanical response of the RF-MEMS tuners is measured with a laser Doppler vibrometer. Fig. 14 shows the measurement setup. Fig. 15 shows the total pull-down and release response of the MEMS fixed–fixed beam tuners when biased with a traditional dc input of 67 V. Fig. 16 shows the measured pull-down time for a variety of input voltages from 65 to 120 V. The measured pull-down switching time ranges from 9 to 22 μs for a device with $V_{pd} = 67$ V, $g_{\rm DC} = 4.8$ μm, and $V_{\rm app} = 120 - 67$ V. The slightly larger $g_{\rm dc}$ may be due to

TABLE IV
PERFORMANCE COMPARISON OF THE ALL-SILICON RF-MEMS TUNABLE RESONATOR WITH EXISTING STATE-OF-THE-ART CAVITY-BASED RESONATORS

	[1]	[7]	[6]	[13]	Authors' previous work [14]	This work	Improvement of authors' previous work [14]
Total frequency tuning [GHz]	$3-5.6$	$1.9-5$	$4.07-5.58$	$11.9-14.2$	$10.7-13$	$15.2-17.8$	NA
Analog tuning range	60.5%	2.6:1	31.3%	13.3%	3.7%	8.2%	$>2.2\times$
Tuner type	Piezoelectric disk	Electrostatic diaphragm	MEMS flat cantilever beam	MEMS highly deflected cantilever beam	MEMS fixed-fixed beam	MEMS fixed-fixed beam	NA
Basic tuning element size	12.7 mm diameter	7 mm diameter	138 μm long 60 μm wide 4 μm thick	1100 μm long 100 μm wide 1.5 μm thick	400 μm long 150 μm wide 1.3 μm thick	185 μm long 20 μm wide 1 μm thick	NA
Number of tuning elements	1	1	4	3	14	75	NA
Electrostatic or Piezoelectric voltage [V]	$\pm$ 210	$0-122$	$0-65$	$0-120$	$0-23$	$0-77$	NA
Resonator Volume [mm^3]	565.5	508.9	700**	180	113.1	54	$>50\%$
Average Resonator Q_u per volume [mm^{-3}]	0.94	0.93	0.57	2.67	7.38	11.4	$>50\%$
Actuation time	$\sim$ 1 ms*	300−500 μs*	60−130 μs [19]	$\sim$ 1 ms***	84 μs	9 μs	$>9\times$
Release/Settling time	$\sim$ 1 ms*	300−500 μs*	60−130 μs [19]	$>$ 5 ms***	112 μs	60 μs	$>1.8\times$
Figure of Merit** [mm^{-3} kg^{-1} V^{-1} s^{-1}]**	1.9×10^{11}	1.97×10^{16}	1.03×10^{20}	2.11×10^{18}	1.83×10^{20}	1.23×10^{22}	$>68\times$

*estimated from tuner size.
**estimated from filter size.
***estimated from tuner size and equations in Section II-D and [16].
****calculated from equation 12 in Section II-E.

postrelease buckling of the fixed–fixed beam. At 65 V, slightly below the measured V_{pd}, a dynamic pull-in phenomenon is observed. In this case, the stepped input bias overshoots the beam into an unstable equilibrium gap height. The hold-down voltage is typically less than the pull-down voltage. The 65-V applied bias falls well within the hold-down voltage range and is sufficient to pull the fixed–fixed beam down to the substrate. The measured switching time is in good agreement with the calculated results using the expression for inertia-limited systems. Table III shows the comparison between the measured and the calculated pull-down switching time.

C. Measured Release Switching Time

Without any voltage input, the release switching time approaches 1 ms as shown in Fig. 17. The reason for the long settling time is the underdamped design and the relatively high Q_m. The measured Q_m and f_{m0} are 32 and 35 kHz, respectively. This is in good agreement with the calculated results. Fig. 18 shows the settling time improvement in the release state of the MEMS tuner in response to both the unit-step and dc-dynamic input bias waveforms as described in Section II-D (please refer to Table II and Fig. 6). The release switching time is measured to be 60 μs to reach 10% of the steady-state gap height. The settling time can potentially be improved through an automated parametric sweep of the waveform parameters in real time. In addition to the settling time improvement, it is readily seen that the biasing waveform excites higher order modes in the fixed–fixed beam. Further investigation with alternative dc-dynamic waveforms will be needed to mitigate these phenomena.

D. Measured Analog Gap Height Switching Time

Fig. 19 shows the measured response of the beam to a typical unit-step input bias waveform. As expected, significant ringing and a long settling time are observed. As discussed in the section on the measured pull-in voltage, the dc-dynamic pull-in voltage is observed for a voltage that typically positions the fixed–fixed beam within the stable analog gap height region. Fig. 20 shows the measured response for unit-step and dc-dynamic exponential input bias waveforms. It is readily observed that the ringing has been significantly suppressed and the settling time has reduced to ~ 50 μs. Fig. 21 shows the improved settling time in the analog gap region for multiple states. As with the release switching time, the ringing can be further suppressed and the settling time reduced by using an automated parametric sweep of the waveform parameters in real time.

V. CONCLUSION

As mentioned in the introductory section of this paper, there are important tradeoffs between quality factor, volume, tuning range, and response speed that need to be explored in designing high-performance resonators. In this paper, we have presented a resonator with an optimized performance with respect to these parameters for a given tuning range. Specifically, the all-silicon tunable resonator exhibits a quality factor of 500–735 from

15.2 to 17.8 GHz for applied biases of 0–77 V. The measured quality factor is 75%–85% of the simulated value. The pull-down and release switching times are 9 and 60 μs, respectively. Table IV summarizes the RF and dynamic performance of the presented resonator and other state-of-the-art cavity-based resonators. Response speed estimates are based on the equations and discussion in Section II-D and [16]. Future work includes investigating the temperature stability and vibration sensitivity of the tunable resonator and employing alternative biasing techniques that utilize wire bonds as opposed to the metal spring in order to facilitate on-chip biasing.

ACKNOWLEDGMENT

The authors would like to thank R. Tung, N. Raghunathan, and the Birck Nanotechnology Center technical staff for the assistance and support. The views, opinions, and/or findings contained in this paper/presentation are those of the authors/presenters and should not be interpreted as representing the official views or policies, either expressed or implied, of the Defense Advanced Research Projects Agency or the Department of Defense. Approved for Public Release, Distribution Unlimited.

REFERENCES

[1] H. Joshi, H. H. Sigmarsson, D. Peroulis, and W. J. Chappell, "Highly loaded evanescent cavities for widely tunable high-*Q* filters," in *IEEE MTT-S Int. Microw. Symp. Tech. Dig.*, Jun. 2007, pp. 2133–2136.

[2] H. Joshi, H. H. Sigmarsson, S. Moon, D. Peroulis, and W. J. Chappell, "High-*Q* fully reconfigurable tunable bandpass filters," *IEEE Trans. Microw. Theory Tech.*, vol. 57, no. 12, pp. 3525–3533, Dec. 2009.

[3] H. Joshi, H. H. Sigmarsson, S. Moon, D. Peroulis, and W. J. Chappell, "High-*Q* narrow-band tunable filters with controllable bandwidth," in *IEEE MTT-S Int. Microw. Symp. Tech. Dig.*, Jun. 2009, pp. 629–632.

[4] S. Moon, H. Sigmarsson, H. Joshi, and W. J. Chappell, "Substrate integrated evanescent-mode cavity filter with a 3.5 to 1 tuning ratio," *IEEE Microw. Wireless Compon. Lett.*, vol. 20, no. 8, pp. 450–452, Aug. 2010.

[5] G. M. Rebeiz, K. Entesari, I. C. Reines, S. Park, M. A. El-Tanani, A. Grichener, and A. R. Brown, "Tuning in to RF MEMS," *IEEE Microw. Mag.*, vol. 10, no. 6, pp. 55–72, Oct. 2009.

[6] S.-J. Park, I. Reines, C. Patel, and G. M. Rebeiz, "High-*Q* RF-MEMS 4–6 GHz tunable evanescent-mode cavity filter," *IEEE Trans. Microw. Theory Tech.*, vol. 58, no. 2, pp. 381–389, Feb. 2010.

[7] X. Liu, L. P. B. Katehi, W. J. Chappell, and D. Peroulis, "High-*Q* tunable microwave cavity resonators and filters using SOI-based RF MEMS tuners," *J. Microelectromech. Syst*, vol. 19, no. 4, pp. 774–784, Aug. 2010.

[8] X. Liu, L. P. B. Katehi, W. J. Chappell, and D. Peroulis, "A 3.4–6.2 GHz continuously tunable electrostatic MEMS resonator with quality factor of 460–530," in *IEEE MTT-S Int. Microw. Symp. Tech. Dig.*, Boston, MA, Jun. 2009, pp. 1149–1152.

[9] W. Irshad and D. Peroulis, "A 12–18 GHz electrostatically tunable liquid metal RF MEMS resonator with quality factor of 1400–1840," in *IEEE MTT-S Int. Microw. Symp. Tech. Dig.*, Baltimore, MD, Jun. 2011.

[10] M. S. Arif, W. Irshad, X. Liu, W. J. Chappell, and D. Peroulis, "A high-*Q* magnetostatically-tunable all-silicon evanescent cavity resonator," in *IEEE MTT-S Int. Microw. Symp. Tech. Dig.*, Baltimore, MD, Jun. 2011, pp. 1–4.

[11] M. S. Arif and D. Peroulis, "A 6 to 24 GHz continuously tunable, microfabricated, high-*Q* cavity resonator with electrostatic MEMS actuation," in *IEEE MTT-S Int. Microw. Symp. Tech. Dig.*, 2012, pp. 1–3.

[12] X. Liu, J. Small, D. Berdy, L. P. B. Katehi, W. J. Chappell, and D. Peroulis, "Impact of mechanical vibration on the performance of RF MEMS evanescent-mode tunable resonators," *IEEE Microw. Wireless Compon. Lett.*, vol. 21, no. 8, pp. 406–408, Aug. 2011.

[13] R. Stefanini, J. D. Martinez, M. Chatras, A. Pothier, V. E. Boria, and P. Blondy, "Ku band high-*Q* tunable surface-mounted cavity resonator using RF MEMS varactors," *IEEE Microw. Wireless Compon. Lett.*, vol. 21, no. 5, pp. 237–239, May 2011.

[14] J. Small, W. Irshad, and D. Peroulis, "A fast high-*Q* X-band RF-MEMS reconfigurable evanescent-mode cavity resonator," in *IEEE MTT-S Int. Microw. Symp. Tech. Dig.*, 2012, pp. 1–3.

[15] H. Joshi, H. H. Sigmarsson, and W. J. Chappell, "Analytical modeling of highly loaded evanescent-mode cavity resonators for widely tunable high-*Q* filter applications," in *Proc. Union Radio Scientifique Int. (URSI)*, Chicago, IL, Aug. 2008.

[16] G. M. Rebeiz, *RF MEMS: Theory, Design and Technology*. New York: Wiley, 2003.

[17] J. Small, A. Fruehling, A. Garg, X. Liu, and D. Peroulis, "DC-dynamic biasing for $> 50\times$ switching time improvement in severely underdamped fringing-field MEMS actuators," *J. Micromech. Microeng.*, vol. 22, no. 12, Nov. 2012, doi:10.1088/0960-1317/22/12/125029.

[18] E. S. Hung and S. D. Senturia, "Extending the travel range of analog-tuned electrostatic actuators," *J. Microelectromech. Syst.*, vol. 8, no. 4, pp. 497–505, Dec. 1999.

[19] A. Grichener, B. Lakshminarayanan, and G. M. Rebeiz, "High-*Q* RF MEMS capacitor with digital/analog tuning capabilities," in *IEEE MTT-S Int. Microw. Symp. Tech. Dig.*, Atlanta, GA, Jun. 2008, pp. 1238–1286.

[20] S. Gong, T. Reck, and N. S. Barker, "A temperature insensitive dc-contact RF-MEMS switch," in *Proc. 40th Eur. Microw. Conf.*, Paris, France, 2010, pp. 1114–1117.

[21] C. D. Patel and G. M. Rebeiz, "A high power (>5 W) temperature stable RF-MEMS metal-contact switch with orthogonal anchors and force-enhancing stoppers," in *IEEE MTT-S Int. Microw. Symp. Tech. Dig.*, Baltimore, MD, Jun. 2011, pp. 1–4.

[22] S.-J. Park, M. A. El-Tanani, I. Reines, and G. M. Rebeiz, "Low loss 4–6 GHz tunable filter with 3-bit high-*Q* orthogonal bias RF-MEMS capacitance network," *IEEE Trans. Microw. Theory Tech.*, vol. 56, no. 10, pp. 2248–2355, Oct. 2008.

Joshua Small (S'11–M'12) received the B.S. degree in electrical engineering from Morgan State University, Baltimore, MD, in 2005 and the Ph.D. degree from Purdue University, West Lafayette, IN, in 2012.

He is currently a Postdoctoral Research Engineer with the Department of Electrical and Computer Engineering, University of California, Davis. His research interests include investigating novel high-*Q* microstructures for reconfigurable radio front ends.

Muhammad Shoaib Arif (S'09) received the B.S. degree in aeronautical engineering from the National University of Science and Technology, Islamabad, Pakistan, in 1999 and the M.S. degree in electrical and computer engineering from Purdue University, West Lafayette, IN, in 2009, where he is currently working toward the Ph.D. degree in electrical and computer engineering.

His research interests include novel RF MEMS devices and micromachined high-*Q* tunable filters for reconfigurable RF front ends.

Adam Fruehling (S'06) received the B.S. degree in electrical engineering from Purdue University, West Lafayette, IN, in 2005, where he is currently working toward the Ph.D. degree in electrical engineering.

His research interests include RF MEMS design, reliability, and monitoring techniques.

Dimitrios Peroulis (S'99–M'04) received the Ph.D. degree in electrical engineering from the University of Michigan, Ann Arbor, in 2003.

He has been with Purdue University, West Lafayette, IN, since August 2003, where he is currently leading a group of graduate students on a variety of research projects in the areas of RF MEMS, sensing and power harvesting applications, as well as RF identification sensors for the health monitoring of sensitive equipment. He has been a Principle Investigator (PI) or a co-PI in numerous projects funded by government agencies and industry in these areas. He is currently a key contributor in two Defense Advanced Research Project Agency (DARPA) projects at Purdue, which focus on very high quality $(Q > 1000)$ RF tunable filters in mobile form factors (DARPA Analog Spectral Processing Program, Phases I, II, and III) and on developing comprehensive characterization methods and models for understanding the viscoelasticity/creep phenomena in high-power RF MEMS devices (DARPA M/NEMS S&T Fundamentals Program, Phases I and II). Furthermore, he leads the experimental program on the Center for the Prediction of Reliability, Integrity and Survivability of Microsystems funded by the National Nuclear Security Administration. In addition, he heads the development of the MEMS technology in a U.S. Navy project (Marines) funded under the Technology Insertion Program for Savings program focused on harsh-environment wireless microsensors for the health monitoring of aircraft engines. He has authored or coauthored over 110 refereed journal and conference publications in the areas of microwave integrated circuits and antennas.

Dr. Peroulis was the recipient of a 2008 National Science Foundation CAREER Award. His students have been the recipients of numerous Student Paper Awards and other student research-based scholarships. He has also been the recipient of eight teaching awards, including the 2010 HKN C. Holmes MacDonald Outstanding Teaching Award and the 2010 Charles B. Murphy Award, which is Purdue University's highest undergraduate teaching honor.